

# Fast Gated Superconducting Nanowire Camera for Multi-Functional Optical Tomograph

Grant Agreement Nº 101099291

**WP 5** 

**D5.2: Liquid phantoms test** 

**Lead Beneficiary: ICFO** 

Due date of deliverable: 31.03.2025

Type and dissemination level: Report, Public





#### **Table of Contents**

Α	bout fas	tMOT	. 1		
E	Executive summary				
Α	Abbreviations				
Li	ist of co	ntributors	. 3		
1	Introd	uction and objectives	. 4		
2	Experimental setup and analysis methods				
3	Valida	ation	. 5		
	3.1	Depth-scanning protocol	. 5		
	3.1.1	Continuous-wave analysis	. 5		
	3.1.2	Time-gated analysis	. 7		
	3.2	X-Y scanning protocol	. 8		
4	Concl	Conclusion9			
5	References1				



#### **List of figures**

gure 1: Normalized electric field autocorrelation functions $(g_1)$ measured during the depth-scanning protocol. Sub-plots A1 and B1 correspond to the raw $g_1$ measured for each depth and the difference between $g_1$ measured with the inclusion $(g'1)$ and $g_1$ measured without any inclusion $(g10)$ respectively taken with a source-detector separation of 0.5 cm. Sub-plots A2 and B2 represent the same data as A1 and B1 but with a source-detector separation of 1.5 cm. Finally, subplots C1 and C2 represent the calculated perturbation (Eq.1).
gure 2: Results from the depth-scanning protocol using $\rho = 1$ cm and a time-gated analysis. In subplot A an example of a measured DTOF and IRF are shown together with the three time-gates that were considered in the time-gated analysis. In subplot B, perturbations calculated from the time-gated $g_1$ curves are shown for all time-gates and at each inclusion depth. Finally, in subplot C, the calculated relative value of flow for each time-gate and all inclusion depths is shown
gure 3: CW analysis of flow over a $1\times1$ cm <sup>2</sup> scanned area (subplot A) and along one axis (subplot B). In subplot A, measurement points are shown in black, the rest of the data is interpolated from the measurement points. The calculated perturbations across one axis for an early and late time gate are shown in subplot C

#### Disclaimer

This document is part of the deliverables from the project fastMOT, which has received funding from the European Union. Views and opinions expressed are however those of the author(s) only and do not necessarily reflect those of the European Union or the European Commission. Neither the European Union nor the granting authority can be held responsible for them.



#### **About fastMOT**

Traditionally, the monitoring of organs and deep body functional imaging is done by ultrasound, X-Rays (incl. CT), PET or MRI. These techniques only allow for very limited measurements of functionality, usually combined with exogenous and radioactive agents. In this project we are developing an innovative light sensing solution, a fast gated, ultra-high quantum efficiency single-photon sensor, to enable multi-functional deep body imaging with diffuse optics.

The new type of sensor is based on superconducting nanowire single-photon detectors that have shown to be ultra-fast and highly efficient. However, until now the active area and number of pixels has been limited to micrometres diameter and tens of pixels. We are using a combination of new techniques to overcome this limit and scale to 10,000 pixels and millimetre diameter.

In addition, we are developing new strategies for performing TD-NIRS and TD-SCOS to use this new light sensor optimally with Monte-Carlo simulations. We will implement the new light sensor in an optical tomograph and achieve a 100x improvement of SNR compared to using existing light sensors. With our Multifunctional Optical Tomograph we will be able to image deep organ and optical structures and monitor functions including oxygenation, haemodynamics, perfusion and metabolism.



## **Executive summary**

The final aim of the multifunctional optical tomograph being developed in the fastMOT project is to non-invasively measure local values of tissue oxygen saturation (StO<sub>2</sub>) by means of time-domain near-infrared spectroscopy (TD-NIRS) and a blood flow index (BFI) by means of time-domain diffuse correlation spectroscopy (TD-DCS) and/or time-domain speckle contrast optical spectroscopy (TD-SCOS). By combining both TD-NIRS with TD-DCS and/or TD-SCOS, the metabolic rate of oxygen (MRO<sub>2</sub>) and the oxygen extraction fraction (OEF) can theoretically be measured. Using the time-domain modalities of the three methods, time-gated parameters can be measured allowing for depth-sensitive measurements.

In this report, we present the results of liquid phantom tests including a small inhomogeneity in flow to explore the feasibility of depth-resolved tomography by means of TD-DCS using the prototype benchtop system outlined in Deliverables 4.1 and 4.2. This report includes the outline, the purpose of the measurements (Section 1), a description of the experimental setup and analysis methods (Section 2) and finally a presentation the results of the experimental measurements (Section 3). We conclude with indications of the future steps which should be taken (Section 4).



# **Abbreviations**

Abbreviation	Definition
TD-NIRS	Time domain near infrared spectroscopy
TD-DCS	Time domain diffuse correlation spectroscopy
TD-SCOS	Time domain speckle contrast optical spectroscopy
DTOF	Distribution of times of flight
IRF	Instrument response function
FWHM	Full-width half-maximum

# **List of contributors**

Institution	Name
ICFO	Lisa Kobayashi Frisk <lisa.kobayashi@icfo.eu></lisa.kobayashi@icfo.eu>
ICFO	Turgut Durduran <turgut.durduran@icfo.eu></turgut.durduran@icfo.eu>
CUSBO	Alberto Dalla Mora <alberto.dallamora@polimi.it></alberto.dallamora@polimi.it>
CUSBO	Laura Di Sieno <laura.disieno@polimi.it></laura.disieno@polimi.it>
CUSBO	Tommaso Palo <tommaso.palo@polimi.it></tommaso.palo@polimi.it>
CUSBO	Antonio Pifferi <antonio.piferri@polimi.it></antonio.piferri@polimi.it>



#### 1 Introduction and objectives

The multifunctional optical tomograph being developed in the fastMOT project aims to non-invasively provide three-dimensional measurements of cerebral blood flow and oxygenation by means of the tomographic counterparts of time-domain diffuse correlation spectroscopy (TD-DCS), time-domain speckle contrast optical spectroscopy (TD-SCOS) and time-domain near-infrared spectroscopy (TD-NIRS) respectively. In this deliverable, we aim to demonstrate the feasibility of tomographic measurements of flow using the detection scheme of the pilot workstations described in D4.1 and the laser source described in D4.2. To this end, we have designed and implemented two protocols with the aim to demonstrate the measurement of a small inhomogeneity in flow using both continuous-wave DCS (CW-DCS) and TD-DCS. The two protocols that have been developed are:

- 1) Depth-scanning protocol: the main objective of this protocol is to evaluate the maximum depth at which the laboratory benchmark is able to detect an inhomogeneity in flow.
- 2) X-Y scanning protocol: the main objective of this protocol is to evaluate whether the laboratory benchmark is able to localize an inhomogeneity in flow.

In order to perform these two protocols, a common basic liquid phantom was used which included a solid silicone inclusion suspended within the liquid. The details of the setup as well as the analysis methods used to evaluate the data are described in the following sections.

## 2 Experimental setup and analysis methods

We have used the workstation available at CUSBO which consists of the detectors described in detail in Deliverable 4.1 and the a laser source for time-domain DCS at fixed wavelength (for more details on the laser source, please refer to Deliverable 4.2). All measurements were taken with the laser operating at 1064 nm and with a repetition rate of 100 MHz. For both the depth-scanning protocol and X-Y scanning protocol, a liquid phantom was prepared consisting of distilled water, Intralipid® and ink solution that was prepared in order to match the optical properties ( $\mu_a = 0.2 \text{ cm}^{-1}$ ,  $\mu'_s = 11 \text{ cm}^{-1}$  at 1064 nm) of a cylindrical silicone inclusion measuring 1 cm in diameter and 1 cm in height. The cylindrical inclusion was suspended horizontally in the liquid phantom by means of a thin fishing line which we assumed was optically transparent. The optical probe consisting of a multimode (MM) source fiber and a single-mode (SM) detector fiber was placed at the top of the surface of the liquid phantom.



In the present deliverable, the CW-DCS analysis pipeline described in Deliverable 5.1 has been expanded to a two-step process. In the first step, time-domain near infrared spectroscopy (TD-NIRS) was used to retrieve the true optical properties of the phantom, namely the absorption coefficient ( $\mu_a$ ) and the reduced scattering coefficient ( $\mu_s'$ ). In the second step, the time-tagged photons were reprocessed using diffuse correlation spectroscopy (DCS) and the optical properties calculated with TD-NIRS. DCS analysis was performed both without considering the sync pulses (i.e. effectively CW-DCS) and with time-gating by taking into account the delay time between sync pulses and diffuse photon detection (i.e. time-domain DCS (TD-DCS)). When retrieving the flow parameter ( $\alpha D_b$ ), using CW-DCS, the method of [1] was used, while when using TD-DCS the method of [2] which includes a correction factor for the effects of the instrument response function (IRF) and the time-gates.

In addition to fitting for  $\alpha D_b$ , perturbations in the electric field autocorrelation function (g<sub>1</sub>) were also calculated. In this case, perturbation was defined by the following equation:

$$perturbation = \frac{\sum_{i=A}^{B} \frac{g'_{1}(\tau_{i})}{g_{1}^{0}(\tau_{i})}}{B-A}$$
 (1)

where in equation 1,  $g'_1$  and  $g^0_1$  are the perturbed and unperturbed values of  $g_1$  respectively.  $\tau$  is the delay time and i is an index. The limits of the summation, A and B are the index values of  $\tau$  which correspond to a specific upper and lower cut-off value of  $g'_1$ . For the purpose of all of the analyses presented in this deliverable, A and B correspond to the indices where  $g'_1$  had a value of 0.8 and 0.2 respectively.

By defining perturbation in this way, perturbation values greater than one indicate slower decays in  $g'_1$  and therefore lower values of flow. Conversely, perturbation values less than one indicate faster decays in  $g'_1$  and therefore higher values of flow.

#### 3 Validation

## 3.1 Depth-scanning protocol

#### 3.1.1 Continuous-wave analysis

The depth-scanning protocol consisted of a set of measurements starting with the solid inclusion suspended at the surface of the liquid and in successive measurements a pre-determined volume of liquid phantom solution was titrated to successively increase the distance from the top surface of the



inclusion to the top surface of the liquid phantom and optical probe by 0.25 cm. The process was repeated nine times to generate a matrix of depth measurements of 0.00, 0.25, 0.50, 0.75, 1.00, 1.25, 1.50, 1.75 and 2.00 cm. Immediately after measuring the inclusion at different depths, the inclusion was carefully removed from the liquid phantom and a separate measurement was taken without the inclusion.

This protocol was repeated twice using two different source-detector separations: one short separation of 1.0 cm and another longer separation of 1.5 cm.

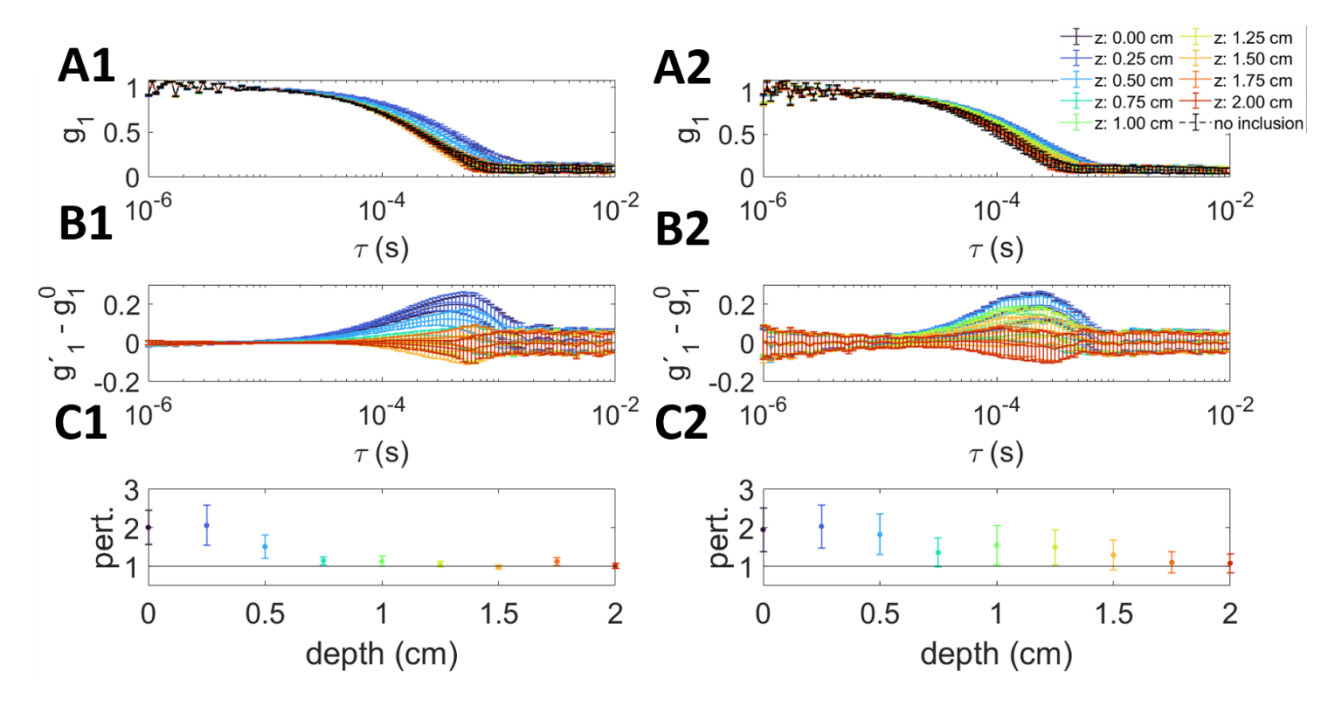


Figure 1: Normalized electric field autocorrelation functions  $(g_1)$  measured during the depth-scanning protocol. Sub-plots A1 and B1 correspond to the raw  $g_1$  measured for each depth and the difference between  $g_1$  measured with the inclusion  $(g'_1)$  and  $g_1$  measured without any inclusion  $(g_1^0)$  respectively taken with a source-detector separation of 0.5 cm. Sub-plots A2 and B2 represent the same data as A1 and B1 but with a source-detector separation of 1.5 cm. Finally, subplots C1 and C2 represent the calculated perturbation (Eq.1).

As seen in Fig. 1 sub-plots A1 and A2, the  $g_1$  curves decay more slowly as the inclusion was closer to the surface of the liquid phantom indicating an overall lower measured value of flow due to the greater sensitivity of the measurement to the solid inclusion. As the inclusion was submerged deeper in the liquid and located further away from the probe, the  $g_1$  curves have a faster decay indicating greater sensitivity to the faster flow of the surrounding liquid phantom compared to the solid inclusion.

In Fig. 1 sub-plots B1 and B2, the difference in  $g_1$  curves with  $(g'_1)$  and without  $(g_1^0)$  the inclusion is shown. In these plots, the difference between  $g_1$  may be appreciated in greater detail. For a short source-detector separation (1 cm, sub-plot B1), a clear difference between  $g'_1$  and  $g_1^0$  is seen for



shallow depths up to approximately 0.5 cm. On the other, for a longer source-detector separation (1.5 cm, sub-plot B2), differences between  $g'_1$  and  $g^0_1$  are visible for depths up to approximately 1.25 cm. These observations partially carry over to the perturbation results shown in sub-plots C1 and C2. In these plots, it is shown that although the average perturbations at depths beyond 0.5 cm is greater for the long source-detector separation (sub-plot C2) compared to the short source-detector separation (sub-plot C1), the measurement is much noisier.

#### 3.1.2 Time-gated analysis

In order to improve depth-resolution and sensitivity to the inclusion, a time-gated analysis was performed on the data taken with  $\rho$  = 1 cm. For this analysis, three time-gates gates were chosen: one "early", one "late", and one "very-late" gate. The three gates did not overlap, and the "early" and "late" gates had a width of 400 ps. The "very-late" gate which was considered had a width of 3000 ns. The gate widths were chosen to be at least 400 ps wide since the full-width half-maximum (FWHM) of the instrument response function (IRF) was measured to be approximately 300 ps. The "very-late" gate had a width of 3000 ns in order to increase the signal to noise ratio (SNR) of this gate which contained a significantly lower number of detected photons.

The gates considered in the analysis are shown in Fig. 2 subplot A together with an example of a measured distribution of time of flight (DTOF) and IRF. The perturbation and derived values of relative flow  $(r\alpha D_b)$  calculated for each time-gate is shown in Figure 2 subplots B and C respectively. All values are relative to the measured value of flow with no inclusion.

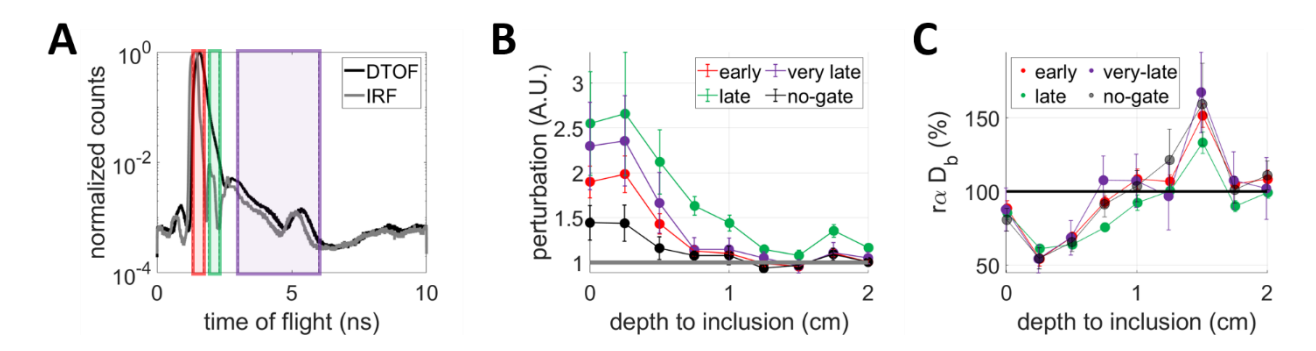


Figure 2: Results from the depth-scanning protocol using  $\rho=1$  cm and a time-gated analysis. In subplot A an example of a measured DTOF and IRF are shown together with the three time-gates that were considered in the time-gated analysis. In subplot B, perturbations calculated from the time-gated  $g_1$  curves are shown for all time-gates and at each inclusion depth. Finally, in subplot C, the calculated relative value of flow for each time-gate and all inclusion depths is shown.

As seen in Figure 2 B and C, all time-gates detected a difference in flow compared to the no-inclusion case, particularly when the depth to inclusion was shallow. The early time-gate demonstrates a clear



differences in both perturbation and  $r\alpha D_b$  compared to the non-inclusion case until a depth of approximately 0.5 cm (subplots B and C). In comparison, the late time-gate has a higher perturbation until a depth of approximately 1 cm and lower  $r\alpha D_b$  until approximately 0.75 cm. We did not see benefits in depth sensitivity in the very-late gate, in particular in the recovery of  $r\alpha D_b$  where in fact the behaviour closely resembled the no-gate case. This may be explained by a volume effect, i.e. even if the late gate photons have a greater sensitivity to the inclusion compared to the earlier gates, the total probed volume was weighted significantly to the liquid compared to the solid inclusion. We note that a spike in  $r\alpha D_b$  was observed in all time-gates when the inclusion was at a depth of 1.5 cm. This observation is most likely a result of an artefact produced by accidentally moving the container containing the liquid phantom.

# 3.2 X-Y scanning protocol

In a full tomographic system, in addition to depth resolution, it is important that perturbations can be reconstructed in the correct x-y plane. For this reason, we performed a second protocol using the same concept of suspending the same cylindrical silicone inclusion in a liquid phantom. In this protocol, the optical probe was once again placed on the surface of the liquid phantom and then scanned across the surface of the phantom using a translational stage and a step-size of 0.25 cm. The starting coordinate (0,0) was estimated as the point where the solid inclusion was directly below the source and detector fibers (within human error). The X-Y scan protocol was for an inclusion depth of 0.25 cm and a source-detector separation of 1 cm. The results of the X-Y protocol are shown in Figure 3.

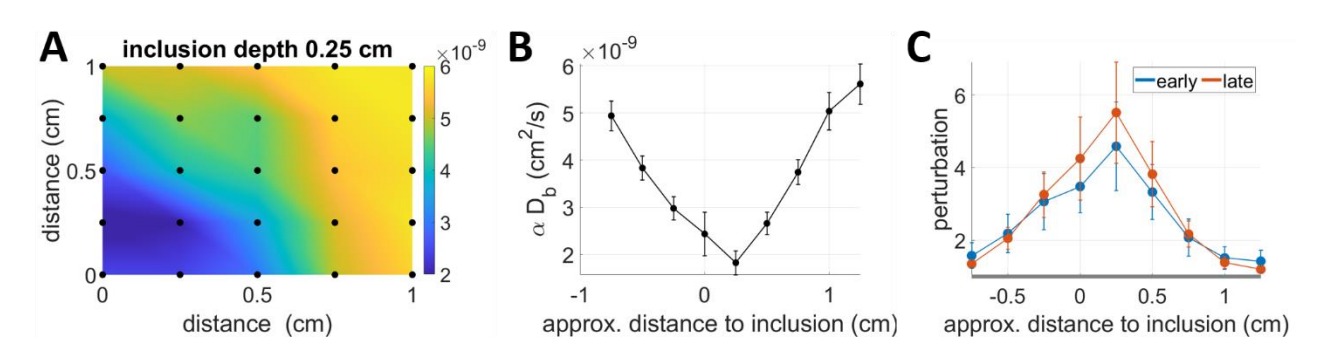


Figure 3: CW analysis of flow over a  $1 \times 1$  cm<sup>2</sup> scanned area (subplot A) and along one axis (subplot B). In subplot A, measurement points are shown in black, the rest of the data is interpolated from the measurement points. The calculated perturbations across one axis for an early and late time gate are shown in subplot C.

As seen in Figure 3, a clear increase in  $\alpha D_b$  was found as the measurement probe was moved a greater lateral distance from the inclusion (subplot A). When scanning the measurement probe along one axis, the lowest value of  $\alpha D_b$  was recorded when the probe was approximately directly above



the inclusion as expected, and increased nearly symmetrically as the probe was scanned laterally across the inclusion (subplot B). Finally, perturbations in  $g_1$  were calculated for both an early and late time-gate. Both time-gates had a width of 400 ps, chosen so that the width of the time-gate was at least as wide as the IRF. As expected from theory, the late time-gate demonstrated a larger perturbation compared to the early time-gate indicating a greater sensitivity to the solid inclusion. The perturbations measured using both the early and late gates have a similar width profile, indicating a similar X-Y localization of the solid inclusion.

#### 4 Conclusion

We have demonstrated the ability of the workstation to detect inhomogeneities in flow using a liquid phantom with a solid inclusion by both a continuous-wave analysis and time-gated analysis. The time-gated analysis offered improvements in depth sensitivity compared to the continuous-wave analysis. However, the improvements in depth sensitivity are somewhat limited. Future work should focus on increasing this depth sensitivity. This may be done through system design, for example by continued analysis of the suitability of the laser or by employing strategies to improve light delivery to increase signal levels particularly in very late gates. Depth sensitivity may also be improved algorithmically by improving analysis methods or through simulations to benchmark optimal pulse widths and gate times.



#### **5** References

[1] Boas, D. A., & Yodh, A. G. (1997). Spatially varying dynamical properties of turbid media probed with diffusing temporal light correlation. JOSA A, 14(1), 192-215.

[2] Colombo, L., Pagliazzi, M., Sekar, S. K. V., Contini, D., Dalla Mora, A, Spinelli, L., ... & Pifferi, A. (2019). Effects of the instrument response function and the gate width in time-domain diffuse correlation spectroscopy: model and validations. *Neurophotonics*, *6*(3), 035001-035001.